

Structure of the self-interstitial in diamond

Hannah E. Smith and Gordon Davies*

Physics Department, King's College London, Strand, London WC2R 2LS, United Kingdom

M. E. Newton

Department of Physics, University of Warwick, Coventry CV4 7AL, United Kingdom

H. Kanda

National Institute for Material Science, 1-1 Namiki, Tsukuba, Ibaraki 305, Japan

(Received 29 August 2003; published 15 January 2004)

We report on a study of the structure of the neutral self-interstitial I^0 in diamond, through the use of uniaxial stress measurements and isotope-substitution effects on the optical absorption lines near 1685 and 1859 meV. The stress perturbations are explicable in terms of a center with D_{2d} symmetry, and the dominant stress-induced perturbations are found to be interactions between the states of the center. The interstate couplings establish that the excited electronic state of the transitions is a doublet, of 5.0 ± 0.1 meV splitting, revealing the existence of another electronic state at I^0 that has not been discussed within existing models of the center. The excited-state doublet couples through B_2 deformations, while the well-known ground-state doublet, whose splitting is measured spectroscopically at 7.6 ± 0.1 meV, is coupled by B_1 deformations of the center. The data are quantitatively consistent with I^0 , in its ground electronic state, tunneling rapidly in a B_1 vibrational mode between equivalent D_{2d} -symmetry configurations, and in its excited electronic state tunneling in a B_2 mode between equivalent C_{2v} -symmetry configurations; in both cases, the motion is sufficiently rapid for I^0 to have the observed effective D_{2d} point group.

DOI: 10.1103/PhysRevB.69.045203

PACS number(s): 61.82.Fk, 78.30.Am, 78.40.-q

I. INTRODUCTION

Diamond is the only elemental semiconductor in which the isolated self-interstitial has been identified. Electron paramagnetic resonance (epr) studies show that the electrically neutral self-interstitial, I^0 , occupies a split $\langle 001 \rangle$ configuration,¹ in agreement with early^{2,3} and recent⁴⁻⁶ theoretical predictions. The same local atomic configuration is predicted, but not yet conclusively identified, for the interstitial carbon atom trapped at a carbon anti-site in SiC.^{7,8} In this paper we combine uniaxial stress and isotope effects to study the structure of I^0 in diamond. We show that a previously unreported electronic state exists. The presence of almost degenerate doublets, and the strong interactions of levels when the center deforms, suggest that the observed D_{2d} symmetry is the mean configuration of two different tunneling motions. Tunneling motion in the ground state is shown to involve a B_1 vibrational mode, and in the excited state it involves a B_2 mode.

The epr-active state of I^0 has spin $S = 1$, and lies about 50 meV above the ground state of the center.¹ The interstitial produces an optical absorption line at 1859 meV, in a transition that originates from the nonparamagnetic ground state, Fig. 1. The intensity of this transition at 77 K has been calibrated in terms of the concentration of the center.¹ A weak absorption line at 1685 meV has also been correlated with the 1859 meV signal.⁹

The optical and epr signals have established that in the limit of low irradiation temperature, the production rate of I^0 is closely equal to the production rate of the neutral vacancy, V^0 , when pure diamonds are irradiated with MeV electrons.¹⁰ When radiation damage is created by electrons at

temperatures greater than about 100 K, a radiation-enhanced migration of I^0 occurs. Approximately two-thirds of the self-interstitials move with a migration energy of ≈ 0.3 eV,¹⁰ possibly causing the long-range migration observed in high-energy electron microscopes.¹¹ There is no known spectroscopic signal associated with the fast-diffusing species. Thermally activated migration of I^0 occurs near 600–700 K, with an activation energy of 1.68 ± 0.15 eV.¹² I^0 is therefore thermally stable at room temperature. The vacancy V^0 is stable to about 900–1000 K. Consequently, I^0 anneals out before V^0 , and it is not known how to create I^0 without V^0 in pure diamond. By using diamonds of controlled isotopic abundance, the 1859 meV line has been shown to involve a local mode of vibration of the center with a quantum of 168.6 meV.¹³ (Throughout, values quoted without qualification are valid for the limit of low temperature and for diamond of natural isotope abundance, 99% ^{12}C .) The 1859 meV line appears to be asymmetric, although its location near the optic mode of V^0 makes its shape difficult to measure, Fig. 1(a). Because the phonon energy is only slightly larger than the cutoff energy of the phonon continuum of diamond at 166 meV,¹⁴ weak coupling between the local mode and the phonon continuum would result in an asymmetric line shape.¹⁵ The apparent asymmetry, together with the proximity of the optic-mode phonon sideband of the neutral vacancy “GR1” transition, complicates measurements on the 1859 meV line. With decreasing temperature, the 1859 meV line strengthens in intensity, and the associated optical absorption line at 1685 meV decreases in intensity. Studies of the 1685 meV line are complicated by the presence of the much stronger absorption from V^0 , and particularly from the GR1 line at 1673 meV [Fig. 1(a)]. From the thermalization effects, the energy sepa-

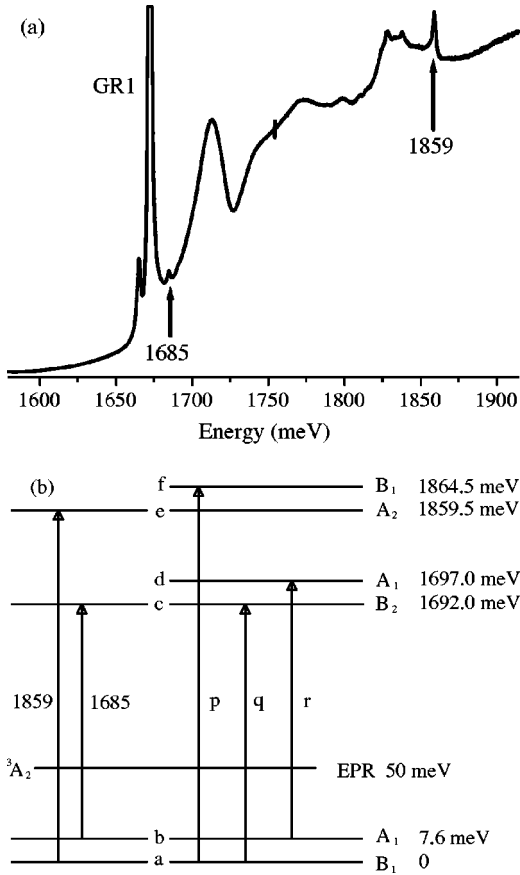


FIG. 1. (a) Absorption spectrum measured at 77 K, showing the 1685 and 1859 meV optical transitions of the self-interstitial, superimposed on the vibronic band of the neutral vacancy. (b) Energy levels of the states involved in optical transitions at the neutral self-interstitial, including the levels “d” and “f” identified in this work, and the epr-active state 3A_2 . Transitions “p,” “q,” and “r” are induced under stress. The irreducible representations of the levels are not uniquely defined in this work. One possible labeling is shown; the set of labels in Table I show all the possible combinations that are indistinguishable in the present experiments.

ration of the lowest levels, “a” and “b,” has been estimated as 6.2 ± 0.5 meV,¹³ decreasing to 5.4 ± 0.4 meV in ${}^{13}\text{C}$ diamond.¹⁵ These values are averages derived from the fits to the data over the temperature range 4 to 200 K. More direct measures of these quantities are given in Sec. III. No luminescence has been detected from any of the transitions of I^0 .

Ab initio calculations of the structure of I^0 predict four electronic states, arising when a one-electron, doubly degenerate state is populated with two electrons.¹⁶ These states transform as 1A_1 , 1B_1 , 1B_2 , and 3A_2 of which the last is the epr-active state. The calculations of the energy of I^0 as a function of *static* distortions give a minimum energy when there is a distortion that transforms as B_1 in the ideal D_{2d} symmetry, resulting in a stable structure with D_2 symmetry.^{6,16} Because the distortion may occur with a positive or negative sign, two equivalent D_2 structures are created from each D_{2d} center, and tunneling between these states was assumed to produce a tunneling splitting of 6 meV.⁶ Independently, a quantum-mechanical description

showed that the relative intensities and energy separation of the 1685 and 1859 meV lines could be explained by a *dynamic* effect in which vibrations of the center mixed the vibronic progressions of two electronic states.¹³ The necessary strength of the interaction was shown to be reasonable and the minimum-energy positions are in close agreement with those later predicted by Goss *et al.*⁶ The symmetry of the deformation was not determined.

Experimental information derived from epr measurements on the atomic configuration of I^0 is inconclusive. The linewidth of the R2 epr transitions is far too great to be due to the electron-electron spin-spin interaction, and the narrow forbidden epr transitions for magnetic field close to $\langle 001 \rangle$ show that the broadening is not caused by short relaxation times. The angular variation of the epr linewidth is consistent with a distribution of values of components of the zero-field splitting term \mathbf{D} about the mean value.¹ Specifically, \mathbf{D} was found to average to effective $\langle 001 \rangle$ axial symmetry, but with a root-mean-square deviation of 2.5% in magnitude and with an rms deviation from the mean direction of 0.6° . One possible cause is motional averaging between two or more extreme values. Motional averaging is characterized by line sharpening at low temperatures, as the system is locked into the equivalent sites, but these measurements are prohibited since the epr signal originates in a state 50 meV above the diamagnetic ground level. Motional narrowing was not observed at high temperatures, to 500 K, but the spin-lattice and spin-spin relaxation times of the R2 signal are extremely short, possibly indicating that motional averaging occurs on a shorter time scale than characteristic times of epr measurements (of about 10^{-10} s).

There is a need to establish experimentally the point group of I^0 , the symmetries of the levels, and the nature of the tunneling motion. In this paper we report and analyze quantitatively the effects of uniaxial stresses on the optical transitions of I^0 : a previous attempt to analyze the uniaxial-stress splitting of the optical transitions was unsuccessful.⁹ In Sec. III we establish that the excited state is a doublet, like the ground state. We show that both doublets are little perturbed in first order by stresses, but that strong interactions occur between their components (Sec. III B). The data can be explained quantitatively using the D_{2d} point group. However, since the interactions can lead to deformations, we briefly investigate in Sec. IV the effects of using the D_2 and C_{2v} point groups. We show in Sec. V A that the coupling within the ground-state doublet is sufficient to produce a dynamic distortion of the center, with the doublet splitting being the result of tunneling between metastable sites of D_2 symmetry. Similar analysis for the excited-state doublet suggests that it would arise from a tunneling motion between sites of C_{2v} symmetry (Sec. V B). The resulting configurational-coordinate diagrams are derived in Sec. V C. The data are summarized in Sec. VI. We begin by outlining the sample preparation and the experimental techniques.

II. EXPERIMENTAL DETAILS

To ensure minimum strains in the samples, and hence small optical linewidths, this work has used synthetic dia-

monds grown by the high-pressure, high-temperature (HPHT) technique with negligible nitrogen concentrations. The samples were selected to contain no inclusions, and, where possible, were taken from single-growth sectors to ensure uniformity.

The samples were x-ray oriented, laser cut, and mechanically polished so that uniaxial stresses could be applied along the $\langle 001 \rangle$, $\langle 111 \rangle$, $\langle 110 \rangle$, and $\langle 112 \rangle$ crystallographic directions. After cutting, the samples were variously irradiated at room temperature with 10^{17} – 2×10^{17} cm $^{-2}$ electrons of 1.5 or 2 MeV, generating between 10^{16} and 2×10^{17} cm $^{-3}$ of I^0 . Optical absorption measurements were taken using a Bruker IFS66 Fourier-transform spectrometer. The Fourier-transform technique allows sufficient signal averaging to detect the weak optical absorption, and easy measurement over a wide photon range of 0.3–2.8 eV. Sample temperatures of between 5 and 77 K allowed the populations of the different ground states of the optical transitions to be optimized. One effect of changing the temperature is that the energies of the transitions change. These effects are small, Fig. 2(b), but have been corrected for. The changes ΔE in energy are readily parametrized, as shown by the lines in Fig. 2(b), by the form $\Delta E = an(T)$, where $n(T)$ is the Bose-Einstein factor, and the fit requires an effective vibrational mode of 16 meV, and $a = \pm 2$ meV.

One disadvantage of using HPHT samples is that they contain very weak optical absorption lines at 1691 and 1693 meV, possibly produced by a defect induced by the solvent-catalyst used in the growth process. The lines have their maximum intensities near 20 K and below 20 K, respectively, Fig. 2. In Sec. III we will report that a transition of I^0 is induced by stress near 1692 meV. This transition has been carefully distinguished from the 1691 and 1693 meV lines by exploiting their polarization and temperature dependencies, and by ensuring that the 1692 meV line annealed out at the same rate as the other lines of I^0 while the 1691 and 1693 meV lines were unaffected by the annealing.

III. UNIAXIAL-STRESS EFFECTS

Uniaxial stresses have been applied at temperatures of ≤ 77 K, where there is no stress-induced re-orientation of the center.¹ The effects of the stresses on the optical transitions near 1685 and 1859 meV are illustrated by the representative spectra of Fig. 3, and the energies of the stress-split components are given in Fig. 4. Lines “p” and “q” are induced by stress, and their temperature dependencies establish that they originate from the level *a* of Fig. 1(b). The polarizations of the components that are present in the limit of low stress are consistent with the 1685 and 1859 meV transitions occurring between nondegenerate states at a tetragonal center.¹⁷ An ideal $\langle 001 \rangle$ split interstitial is a tetragonal center with the D_{2d} point group. Since the stresses used here only induce strains of less than 0.2%, it is sufficient to write the stress-induced change to the Hamiltonian in terms linear in the stress. We define the stress tensor components s_{ij} in terms of the crystal’s Cartesian axes *x*, *y*, *z*. As a representative orientation of I^0 , we choose one with the two interstitial atoms oriented along $[001]$ which is defined as

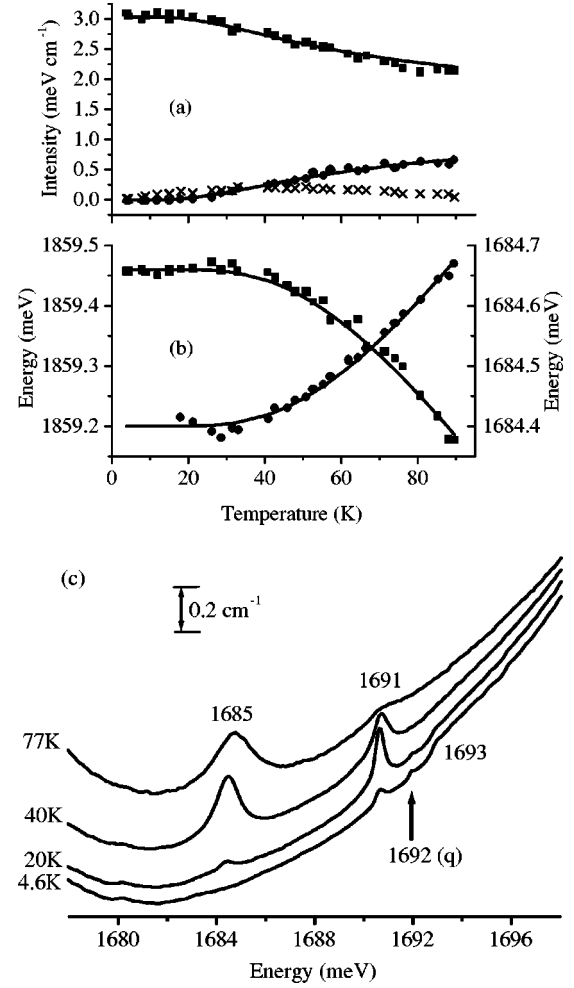


FIG. 2. (a) Intensities as functions of temperature for the 1859 meV line (squares) and the 1685 meV line (dots) of I^0 , and for the 1691 meV line of an unrelated defect (crosses). The lines are calculated assuming a Boltzmann distribution in the ground states “a” and “b,” assumed split by 7.6 meV, Sec. III A. (b) Peak energies as functions of temperature for the 1859 meV line (squares) and 1685 meV line (dots). The lines are empirical fits as described in Sec. II. (c) Absorption spectra showing the 1685, 1691, 1692, and 1693 meV lines at representative temperatures without an applied stress. The spectra have been displaced for clarity. The marker indicates the scale of the absorption coefficient.

the *z* axis. The electric dipole moment of the transitions is oriented parallel to this *z* axis. In D_{2d} symmetry, the perturbation is

$$\Delta V = \hat{a}_1 s_{zz} + \hat{a}'_1 (s_{xx} + s_{yy}) + \hat{b}_1 (s_{xx} - s_{yy}) + \hat{b}_2 s_{xy} + \hat{e}_x s_{yz} + \hat{e}_y s_{xz}. \quad (1)$$

The operators \hat{a}_1 and \hat{a}'_1 transform under the operations of D_{2d} as A_1 , \hat{b}_1 as B_1 , etc. They act on the states of the interstitial.

A. Identification of the states

The stress-induced transition *p* in Figs. 1, 3, and 4 establishes that there is a previously undetected level at 1864

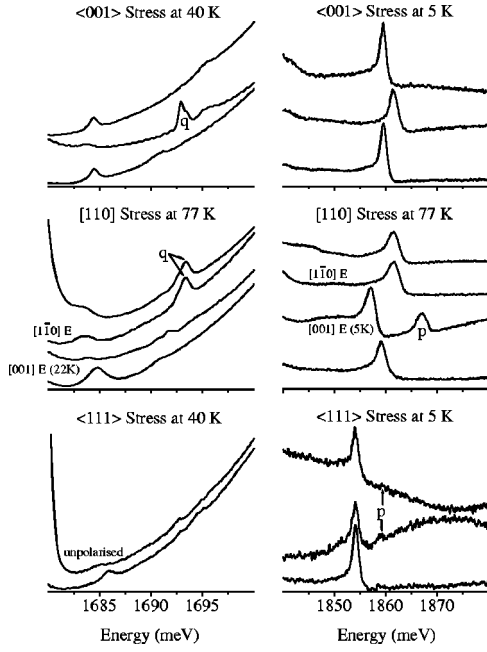


FIG. 3. The effects of stress on the absorption spectra near 1685 meV (left column) and 1859 meV (right column), for stresses applied along the $\langle 001 \rangle$ axis (top row), the $\langle 110 \rangle$ axis (middle row), and the $\langle 111 \rangle$ axis (bottom row). In each diagram the lowest spectrum is at zero stress, and the top spectrum was recorded with an applied stress and with electric vector \mathbf{E} parallel to the stress axis. The middle spectrum was recorded under stress and with \mathbf{E} perpendicular to the stress axis, with the specific directions shown for $[110]$ stress. For $\langle 111 \rangle$ stress, the spectra were measured in a small ^{13}C sample, and to increase the signal-to-noise ratio the stressed spectrum for the 1685 meV region is shown unpolarised. To optimize the signals, the spectra were measured at the temperatures indicated.

meV. (Throughout, the energies of all states of I^0 are quoted relative to the ground state a .) Transitions to it from the lowest energy level a are only induced when the stress tensor component s_{xy} in Eq. (1) is nonzero. This result establishes that states e and f in Fig. 1(b) are only coupled by B_2 perturbations, which lower the symmetry from D_{2d} to C_{2v} . To identify the nature of the final state f of the 1864 meV line we have applied stress along the $\langle 111 \rangle$ axis to a crystal made of 99% ^{13}C , so that the frequencies of all the modes of vibration of I^0 are $\sqrt{12/13}$ of those in normal carbon. The induced line p is down-shifted by 5 meV relative to its energy with natural isotopic abundances, Fig. 4, consistent with its being a one-phonon sideband.

To discuss the nature of the states we will use the Born-Oppenheimer approximation, and will justify this use in Sec. V B. We know that state e is a one-phonon level of state c , and so e will be written as a Born-Oppenheimer product of an electronic part ϕ_c and a one-phonon state $\chi_{j,1}$ in the j th mode of vibration of the center. The state f can either involve the same electronic state and a different mode of vibration, $\phi_c\chi_{k,1}$, or a different electronic state ϕ_x and the same phonon state, $\phi_x\chi_{j,1}$. However, typically stresses produce negligible perturbations on local mode states compared to their effects on electronic states: an explicit example in diamond

involving a phonon of very similar energy to that of the self-interstitial is the “H2” optical band.¹⁸ It is unlikely that the strong stress-induced interaction of states e and f occurs through coupling of two vibrational modes. We conclude that the states e and f are one-phonon levels, involving the same mode of vibration, of two zero-phonon states, denoted c and d on Fig. 1(b). This implies that the splitting of c and d is also close to 5.0 meV, fixing the previously unknown state d at 1697.0 meV.

Direct evidence for the postulated state d comes from noting that since the one-phonon states e and f couple through B_2 stresses, and since the coupling is mediated via the electronic components of those states, rather than their vibrational part, the “zero-phonon” levels c and d will also mix through B_2 stresses. We therefore predict that under $\langle 110 \rangle$ stress, when states c and d are mixed, a transition should be induced between states b and d , with a zero-stress energy near 1690 meV. To observe this weak line requires thermal population of the state b but also low thermal line broadening, and so a measurement temperature of 22 K has been used. We have noted the need to exclude carefully the weak absorption lines at 1691 and 1693 meV resulting from independent optical transitions (Sec. II). The expected transition between b and d is observed, with a low-stress energy of 1689.7 ± 0.3 meV. The existence of state d is therefore verified.

From the appearance of the induced transition “ q ,” at 1692.0 ± 0.1 meV, and the curvature of the shift rates in Fig. 4, we observe that the two lowest-energy states a and b interact only when there is a nonzero component in Eq. (1) of the stress term $s_{xx} - s_{yy}$. States a and b are therefore coupled by a perturbation that transforms as B_1 , which lowers the symmetry from D_{2d} to D_2 . This induced transition is to the same final state c as the “1685 meV” transition [whose precise energy is 1684.4 meV in the limit of low temperature, Fig. 2(b)]. Consequently we can now make a direct spectroscopic measurement of the energy difference of a and b ; the ground-state splitting is 7.6 ± 0.1 meV, in the limit of low temperature. This value fits the measured temperature dependence of the intensities of the 1685 and 1859 meV lines, Fig. 2(a).

The one ^{13}C sample available here has been stressed along its $\langle 112 \rangle$ axis to induce the a to c transition. Its energy extrapolated to zero stress is 1692.9 ± 0.1 meV. In ^{13}C , the 1685 meV line is shifted to 1685.5 meV, Fig. 4, giving an a to b separation of 7.4 ± 0.2 meV in ^{13}C .

We have established from the number of stress-split components and their polarizations that the optical transitions are consistent with a z -oriented dipole in a center of D_{2d} symmetry, between nondegenerate orbital states. The stress data do not allow us to determine unambiguously the irreducible representations of the levels. Referring to Fig. 1(b), suppose that state a transforms as B_1 in D_{2d} symmetry. Then, since b couples to a through B_1 perturbations, b would transform as A_1 . Optical transitions occur from a to e and from b to c under $z \equiv B_2$ polarization, and so e transforms as A_2 and c as B_2 . Since e is a one-phonon sideband of c , the phonon transforms as B_1 . The coupling of e to f is through B_2 perturbations, and so since e transforms as A_2 , f transforms as B_1 .

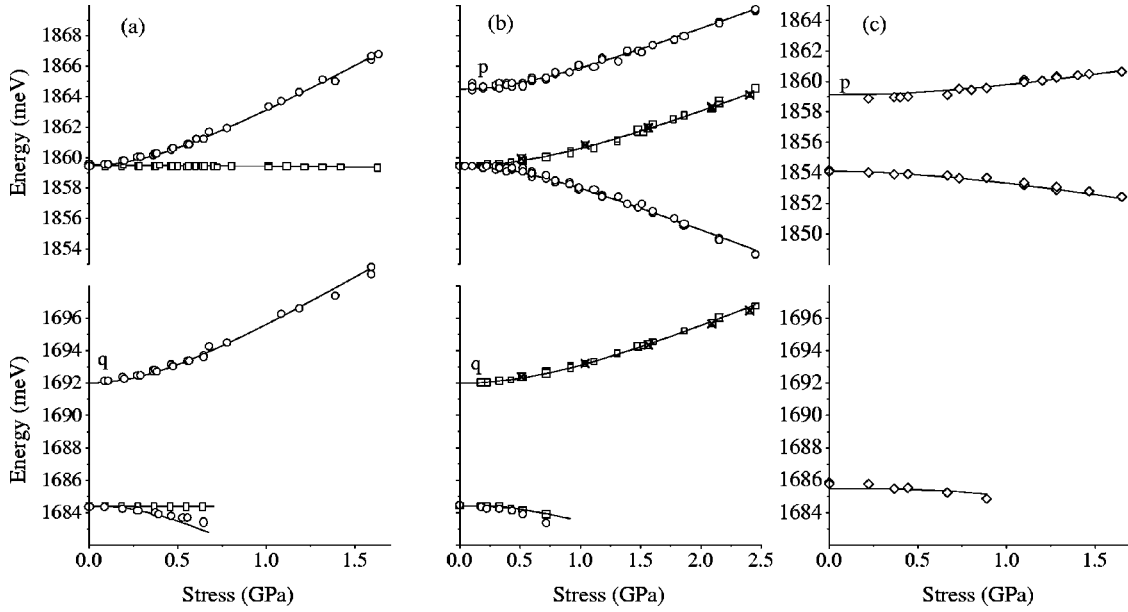


FIG. 4. The energies of the optical transitions as functions of stresses applied along (a) the $\langle 001 \rangle$ axis, (b) the $\langle 110 \rangle$ axis, and (c) the $\langle 111 \rangle$ axis. Data recorded with light polarized parallel to the stress axis are shown by squares, and those with perpendicular polarization by circles. For $[110]$ stress, the circles show specifically the perpendicular polarization with electric vector $\mathbf{E} \parallel [001]$ and the crosses show $\mathbf{E} \parallel [1\bar{1}0]$. The $\langle 111 \rangle$ data were taken using a small ^{13}C sample, and to increase the signal-to-noise ratio they were recorded with unpolarized light. The lines are calculated as in Sec. III, with the assumption that the shift rates are independent of the isotope.

Since c transforms as B_2 , and c and d couple through B_2 perturbations, d transforms as A_1 . The sequence of levels a – f is *unambiguously determined once one level is fixed*. However, the choice of that level is arbitrary, and all four sequences listed in Table I are indistinguishable in the experiments reported here.

B. Quantitative analysis

Each level is perturbed in first order by the stresses that transform as A_1 in Eq. (1). The levels a and b are coupled by the B_1 stresses. The perturbations to the energies of states a and b are therefore given by the eigenvalues of the matrix,

$$\begin{pmatrix} A_1^a s_{zz} & B_1^{ab}(s_{xx} - s_{yy}) \\ +A_2^a(s_{xx} + s_{yy}) & E_b + A_1^b s_{zz} \\ B_1^{ab}(s_{xx} - s_{yy}) & +A_2^b(s_{xx} + s_{yy}) \end{pmatrix}, \quad (2)$$

where E_b is the zero-stress energy of state b relative to state a . The matrix elements are defined as $A_1^a = \langle a | \hat{a}_1 | a \rangle$, $A_2^a = \langle a | \hat{a}'_1 | a \rangle$, $A_1^b = \langle b | \hat{a}_1 | b \rangle$, $A_2^b = \langle b | \hat{a}'_1 | b \rangle$, and $B_1^{ab} = \langle a | \hat{b}_1 | b \rangle$.

The perturbations of states e and f are given by a very similar matrix, but with the B_2 coupling,

$$\begin{pmatrix} E_e + A_1^e s_{zz} & B_2^{ef} s_{xy} \\ +A_2^e(s_{xx} + s_{yy}) & E_f + A_1^f s_{zz} \\ B_2^{ef} s_{xy} & +A_2^f(s_{xx} + s_{yy}) \end{pmatrix}, \quad (3)$$

TABLE I. Consistent labeling of the levels. The experimental data in the paper are consistent with four combinations, for the six energy levels of Fig. 1(b). States “ e ” and “ f ” involve one B_1 phonon of the levels “ c ” and “ d .” The point group is D_{2d} . States “ a ” and “ b ” always couple through B_1 perturbations, and the pairs “ c ” and “ d ,” and “ e ” and “ f ,” through B_2 .

| State | | | | |
|---------|-------|-------|-------|-------|
| “ a ” | B_1 | A_1 | A_2 | B_2 |
| “ b ” | A_1 | B_1 | B_2 | A_2 |
| “ c ” | B_2 | A_2 | A_1 | B_1 |
| “ d ” | A_1 | B_1 | B_2 | A_2 |
| “ e ” | A_2 | B_2 | B_1 | A_1 |
| “ f ” | B_1 | A_1 | A_2 | B_2 |

and the perturbation of the corresponding zero-phonon states c and d are given exactly as in Eq. (3) but with the initial energies E_c and E_d , and matrix elements $A_1^c \dots A_2^d$ and B_2^{cd} . To reduce the number of unknown stress parameters we recall that state e is the one-phonon sideband of state c , and that f is the sideband of d . Therefore we expect that the corresponding stress parameters will be equal ($A_1^e = A_1^c \dots$). Further, since optical measurements only monitor the energy differences between the initial and final states, we may set each of the first-order stress parameters of the excited states equal to zero ($A_1^c = A_1^d \dots = 0$) and incorporate their effects in the ground-state parameters. Consequently,

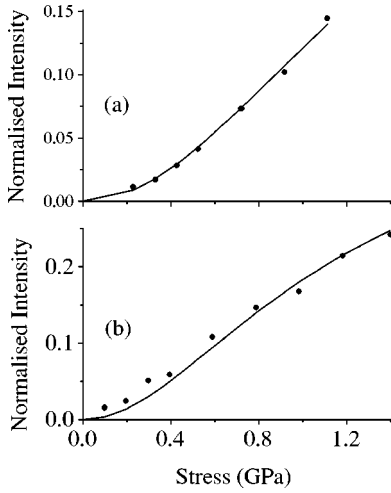


FIG. 5. Points show the measured absorption strengths of (a) the 1692 meV line and (b) the 1864 meV line, both induced by stresses along the $\langle 110 \rangle$ axis at a temperature of 5 K. In (a), the absorption is normalized relative to the absorption that the 1685 meV line would have at zero stress with its initial state fully populated. In (b), the absorption is normalized relative to the 1859 meV line with zero stress at 5 K. The lines are the intensities predicted from the theory of Sec. III B.

there are only six unknown parameters, A_1^a , A_2^a , A_1^b , A_2^b , B_1^{ab} , and B_2^{cd} . All the data taken with both ^{12}C and ^{13}C samples may be used simultaneously, since the elastic constants of diamond are independent of isotopic content at this level of accuracy.¹⁹ A least-squares fit to the stress data yields $A_1^a=0.1$, $A_2^a=0.1$, $A_1^b=0.0$, $A_2^b=-0.5$, $B_1^{ab}=6.3$, and $B_2^{cd}=6.1$ meV GPa⁻¹, with an uncertainty of $\approx \pm 0.5$ meV GPa⁻¹.

We note that, very unusually, all the first-order stress parameters are negligible compared to the coupling terms. This complication, together with measurements constrained by dispersive spectroscopy to be over very limited spectral ranges and the weakness and broad nature of the induced lines at the temperature of the measurements, is the likely reason for the failure to explain the early stress measurements on the self-interstitial.⁹

Knowing now the eigenvectors of Eqs. (2) and (3) for the perturbed states, the intensity of the stress-induced optical transitions may be calculated as a function of stress, relative to the intensity at zero stress of the allowed transitions. The results are in satisfactory agreement with observation, Fig. 5, further confirming the model.

IV. INTERPRETATION AS A STATICALLY DISTORTED CENTER

Relaxation of the $\langle 001 \rangle$ split interstitial by a B_1 distortion leads to D_2 (rhombic I) symmetry. We consider next if the stress data can be consistent with that symmetry. In D_2 symmetry, using a representative orientation as defined for Eq. (1),

$$\Delta V = \hat{a}_1 s_{zz} + \hat{a}_1' s_{xx} + \hat{a}_1'' s_{yy} + \hat{b}_1 s_{xy} + \hat{b}_2 s_{xz} + \hat{b}_3 s_{yz}. \quad (4)$$

Again, the operators \hat{a}_1 , \hat{a}_1' , \hat{a}_1'' transform as A_1 , \hat{b}_3 as B_3 , etc.

Detailed analysis shows that the stress data can be fitted, since the first-order coupling is negligible, but only if a further constraint is introduced—that the interactions of the components of the ground-state doublet a , b are equal and opposite under s_{xx} and s_{yy} stresses, so that they cancel when these stresses are equal. The ground states mix under $s_{xx} - s_{yy}$ stress which transforms as an A_1 perturbation, so the states a and b must have the same symmetry in this point group. Consequently, the 1692 meV transition q is a symmetry-allowed dipole transition and so must have an accidentally near-zero transition probability at zero stress.

The coupling through B_2 perturbations lowers the symmetry from D_{2d} to C_{2v} . A representative center in this point group has its primary (C_2) axis parallel to $[001]$, and two reflection planes normal to $[110]$ and to $[\bar{1}10]$. It is therefore convenient to take the Z axis to be along $[001]$ and the X and Y axes to be along $[110]$ and $[\bar{1}10]$, respectively, the perturbation produced by stress is then

$$\Delta V = \hat{a}_1 s_{zz} + \hat{a}_1' s_{xx} + \hat{a}_1'' s_{yy} + \hat{a}_2 s_{xy} + \hat{b}_1 s_{xz} + \hat{b}_2 s_{yz}, \quad (5)$$

where again the operators transform as indicated by their labels. Again, since the first-order coupling is negligible, the stress data can be fitted. In this case the interactions of the components of the excited state doublet c , d are required to be equal and opposite under s_{xx} and s_{yy} stresses. The excited states mix under $s_{xx} - s_{yy}$ stress (s_{xy} if x and y are the crystal axes as before) which transforms as an A_1 perturbation, so the states c and d must have the same symmetry in this point group. Consequently, the 1864 meV transition p is a symmetry-allowed dipole transition and so must have an accidentally near-zero transition probability at zero stress.

We show in Sec. V that the origin of the doublets can be readily explained if the mean symmetry is D_{2d} and tunneling occurs between the distorted configurations. On the principle of adopting the simplest description, the D_{2d} point group is therefore preferred.

V. ORIGIN OF THE STATES

The uniaxial-stress data have established that the effective symmetry of I^0 as seen optically is D_{2d} . The irreducible representations (IRs) of the states are as shown by the example in Fig. 1(b), or any of the combinations in Table I. Whichever combination is used, two spin-zero states of the same IR are required. This observation contrasts with current theoretical constructs of the electronic states, where two spin-zero states of the same IR cannot be produced by populating a doubly degenerate one-electron state with two electrons.¹⁶ In the next two sections we will investigate the facts that both the ground, a and b , and excited states, c and d , are split by a few meV, and that both pairs are almost equally coupled by stresses of, respectively, B_1 and B_2 symmetries.

A. The low energy doublet a, b

The ground-state splitting of $\Delta E \approx 7$ meV has been described in terms of the tunneling splitting as the self-interstitial moves between equivalent distorted configurations.^{6,13} The tunneling time, $\Delta \tau \approx \hbar / \Delta E \approx 10^{-13}$ s is sufficiently short that the observed symmetry would be the mean, D_{2d} , as observed. It has been shown that the shape of the spectrum (a doublet ground state, with a very weak zero-phonon line at 1685 meV, a stronger one-phonon sideband, and negligible higher-order phonon-sidebands) can be fitted quantitatively in terms of a coupling between the vibronic progressions of two electronic states.¹³ The model assumed two electronic states, of wave functions ψ_a and ψ_b with ψ_b an energy E_0 above ψ_a . Born-Oppenheimer products $\psi_a \chi_n(Q)$ and $\psi_b \chi_m(Q)$ were formed using harmonic-oscillator wave functions $\chi_n(Q)$ for the n th quantum state, Q being the coordinate of the local vibrational mode. These states were assumed to be coupled by a term $\hat{c}Q$ linear in the vibrational coordinate. It couples $\psi_a \chi_n(Q)$ to $\psi_b \chi_{n+1}(Q)$, with a magnitude

$$\int dr dQ \chi_n^*(Q) \psi_a^*(r) \hat{c} Q \psi_b(r) \chi_{n+1}(Q) = c \sqrt{\frac{\hbar}{m\omega}} \sqrt{\frac{n+1}{2}}. \quad (6)$$

For coupling of $\psi_a \chi_n$ to $\psi_b \chi_{n-1}$, $(n+1)$ in the square root is replaced by n . To fit the energy separation of the observed doublet a and b , Sec. III A, and the relative intensities of the 1685 and 1859 meV lines one requires

$$E_0 = 250 \pm 50 \text{ meV}, \quad c \sqrt{\frac{\hbar}{m\omega}} = 325 \pm 15 \text{ meV}. \quad (7)$$

We can now estimate the strength of c independently from the measured coupling B_1^{ab} . There are two steps in the calculation. First we recognize that the measurement of B_1^{ab} is on two particular vibronic levels, $|a\rangle$, $|b\rangle$, while c is defined in terms of the parent electronic states ψ_a and ψ_b . The states are related by

$$\begin{aligned} |a\rangle &= \sum_{n=0}^{\infty} c_{an} \psi_a \chi_n + \sum_{m=0}^{\infty} c_{bm} \psi_b \chi_m, \\ |b\rangle &= \sum_{n=0}^{\infty} d_{an} \psi_a \chi_n + \sum_{m=0}^{\infty} d_{bm} \psi_b \chi_m. \end{aligned} \quad (8)$$

The measured coupling is then

$$\begin{aligned} B_1^{ab} = \langle b | \hat{b}_1 | a \rangle &= \sum_{n=0}^{\infty} c_{an} d_{bn} \int dr \psi_a^* \hat{b}_1 \psi_b \\ &+ \sum_{m=0}^{\infty} c_{bm} d_{am} \int dr \psi_b^* \hat{b}_1 \psi_a. \end{aligned} \quad (9)$$

The eigenvectors $c_{an}, c_{bm}, d_{an}, d_{bm}$ are known explicitly from the secular matrix of which Eq. (6) gives the off-

diagonal terms and the diagonals are simply $(n + \frac{1}{2})\hbar\omega$ and $E_0 + (m + \frac{1}{2})\hbar\omega$. With the parameters of Eq. (7),

$$\langle b | \hat{b}_1 | a \rangle = r \int dr \psi_a^* \hat{b}_1 \psi_b, \quad \text{where } r = 0.96. \quad (10)$$

The ratio r is equivalent to a Ham reduction factor in Jahn-Teller theory,²⁰ where it may differ very significantly from unity. In this problem, with the strong coupling and large energy separation E_0 , $r \approx 1$.

The second stage in the calculation is to convert the stress response, $\int dr \psi_a^* \hat{b}_1 \psi_b$, into a response per unit displacement in the mode Q . The conversion involves the combination of elastic constants ($c_{11} - c_{12}$), which has the value for perfect diamond of 953 GPa;¹⁹ the value near Γ^0 is likely to be higher as a result of the local stiffening of the lattice expected from squeezing the extra atom into the available space.²¹ To convert the movement Q into a strain, we assume that the appropriate scaling length is the bond length, $l = 0.154$ nm. Then

$$c \geq \frac{c_{11} - c_{12}}{lr} \int dr \psi_a^* \hat{b}_1 \psi_b, \quad (11)$$

predicting $c \sqrt{\hbar/m\omega} \geq 190$ meV. The lower limit is within a factor of 2 of the required value, which suggests that the vibronic model is reasonable.

Additionally, the vibronic model proposed in Ref. 13 required that there was no first-order coupling of the local mode to each state, i.e., $\int dr \psi_a^* \hat{b}_1 \psi_a \approx 0$, and likewise for ψ_b . This is confirmed by the negligible size of the first-order stress parameters, Sec. III. It is not possible to test the model further since, for example, we do not know the energy levels of the next vibronic levels above a and b , since the Γ^0 center is nonluminescent.

B. The high-energy doublet c, d

States c and d have a similar splitting to a and b , and the same magnitude of stress-induced coupling, $B_1^{cd} \approx B_2^{ab}$. This similarity implies some “coincidence” in the nature of the pairs of levels. In contrast to the ground states, the one-phonon levels e and f can be observed. They are separated by 5 meV, the same as the zero-phonon levels c and d . At first sight, this result is very unexpected, since the barrier potential seen by the one-phonon levels is expected to be much smaller than that for the zero-phonon levels. However, states c and d couple through B_2 perturbations, not B_1 as for the ground state. If there is a vibronic coupling of two electronic states to produce c and d , it will be through a B_2 phonon. This mode is independent of the B_1 mode, in the harmonic approximation, and the two vibronic deformations can be treated independently. (This is why states e and f could be written as simple Born-Oppenheimer products of the B_1 mode and an “electronic” part ϕ_c or ϕ_d , where we now see that the electronic part can be a linear combination as in Eqs. (8) and (9), but involving the B_2 mode.) In this model, states c and d are zero-phonon states of both the B_1 and B_2 modes, and are split by the tunneling motion produced by the B_2

mode. States e and f have one phonon in the B_1 mode but zero phonons in the B_2 mode, and so are split by the same amount as c and d , as observed. The coupling to the B_2 mode can be described using the theory of Sec. V A, with the elastic constants $(c_{11}-c_{12})$ replaced by c_{44} , which has a similar magnitude [61% of $(c_{11}-c_{12})$], leading to very similar potential surfaces in the ground and excited states.

C. The configurational surface of I^0

A B_1 mode transforms as x^2-y^2 , as in Eq. (1), and lowers the symmetry to D_2 , while B_2 transforms as a shearing motion xy , and lowers the symmetry to C_{2v} . Density-functional calculations predict a saddle point in the B_1 vibrational mode in D_{2d} symmetry.⁶ From the curvature of the potential surface near the D_2 minima, this mode appears to have a quantum slightly greater than the cutoff of diamond,⁶ in agreement with the experimental value of 168.6 meV. Similar calculations to those reported in Refs. 6 and 16, but with a larger cluster of 124 carbon atoms, predict that I^0 has three other local vibrational modes.²² The two modes of highest frequency transform as A_1 and E . A third transforms as B_2 , and is predicted to have an energy of 1143 cm^{-1} . The calculations underestimate vibrational frequencies near the Raman energy, and plausible scaling regimes place this mode $\approx 10 \text{ meV}$ above the Raman energy.

In the electronic ground states of I^0 , the B_2 mode produces no coupling, and so the potential surface is parabolic in that mode. The coupling to the B_1 mode produces a double-minimum shape resulting from two electronic states coupled by the mode. The adiabatic potential surfaces V are given by the solutions of

$$\begin{pmatrix} \frac{1}{2}m_1\omega_1^2Q_1^2 & cQ_1 \\ +\frac{1}{2}m_2\omega_2^2Q_2^2-V & \\ & E_0+\frac{1}{2}m_1\omega_1^2Q_1^2 \\ cQ_1 & +\frac{1}{2}m_2\omega_2^2Q_2^2-V \end{pmatrix} = 0. \quad (12)$$

Here, the suffix 1 refers to the B_1 mode, and 2 to the B_2 mode, m to the mass of the mode and ω its angular frequency. E_0 is the energy separation of the electronic states at $Q_1=Q_2=0$. Schematically, the configurational surface is as in Fig. 6, where the mass of the modes is set to the mass of a carbon atom, and the B_2 mode has been arbitrarily assigned a quantum of 175 meV, since we have no information on the quantum, its value is not critical. The effect of the coupling to the B_1 mode is to lower the energy minimum in the configurational plot by 0.2 eV, taking it below the energy of the 3A_2 epr-active state.

In the excited states of I^0 , we have seen that the coupling is through the B_2 mode, and so here the B_1 mode is parabolic and the B_2 mode shows the double minima, Fig. 6. For illus-

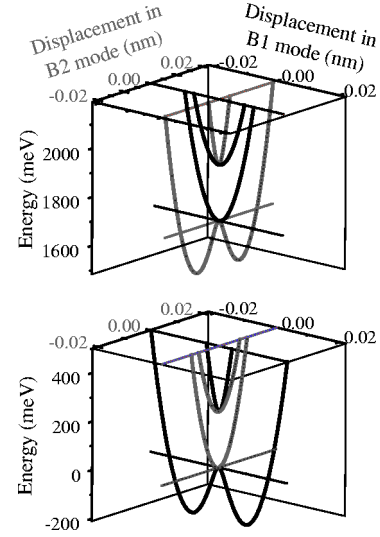


FIG. 6. Schematic configurational-coordinate plots. The lower figure is for the electronic ground states, where tunneling occurs in the B_1 mode and not in the B_2 mode. The parameters used are given in the text. The upper plot is for the electronic excited states, where tunneling occurs in the B_2 mode but not in the B_1 mode.

trative purposes the potential surfaces are drawn using Eq. (12) with cQ_1 replaced by cQ_2 .

There is an intriguing parallel in 3C SiC, where density-functional theory calculations on the interstitial-carbon—carbon-antisite defect predict similar local modes of A_1 , E , and B_2 symmetries as for I^0 , but for this center there is no B_1 local vibrational mode.²³ One consequence of our vibronic model is that in the absence of a B_1 local mode, the epr-active triplet state would be the ground electronic state, as predicted for the interstitial-carbon—carbon antisite in SiC.²³

VI. SUMMARY

We have shown that in the ground state of the center, the neutral $\langle 001 \rangle$ split interstitial effectively has the ideal symmetry of D_{2d} , like the paramagnetic state 50 meV above the ground state. We have shown that the stress perturbations arise predominantly through interactions within the ground-state doublet and within the excited-state doublet. To our knowledge the existence of the excited-state doublet was not realized before this work. The doublets can be understood, in a way that is fully consistent with the stress data, in terms of tunneling between two equivalent minima of D_2 symmetry in the ground state, and two equivalent minima of C_{2v} symmetry in the excited state.

Our model requires that two pairs of electronic states, one for the ground state and one for the excited state, interact through the vibronic coupling mechanism with equal strengths. In other semiconductors, where we can describe electronic states in terms of a bound exciton, it is possible to have one set of energy levels of the hole duplicated by an independent set of levels from the electron.²⁴ The challenge to theory is now to define the origin of the interacting states, and to determine the properties of the different modes of vibration of I^0 .

ACKNOWLEDGMENTS

We thank Chris Kelly, Andy Taylor, Samantha Quinn, and Jacques Jones of the Diamond Trading Company Research Center for sample preparation and characterization, Alison

Mainwood and Karl Johnston for helpful discussions, and Phil Buisson for assistance with preparing the manuscript. This work was funded by EPSRC Grant No. GR/M77826/01, and H.S. thanks EPSRC and the DTC Research Center for financial support.

*Corresponding author. Email address: gordon.davies@kcl.ac.uk

- ¹D.C. Hunt, D.J. Twitchen, M.E. Newton, J.M. Baker, T.R. Anthony, W.F. Banholzer, and S.S. Vagarali, *Phys. Rev. B* **61**, 3863 (2000).
- ²C. Weigel, D. Peak, J.W. Corbett, G.D. Watkins, and R.P. Messmer, *Phys. Rev. B* **8**, 2906 (1973).
- ³A. Mainwood, F.P. Larkins, and A.M. Stoneham, *Solid-State Electron.* **21**, 1431 (1978).
- ⁴L.H. Li and J.E. Lowther, *J. Phys. Chem. Solids* **58**, 1607 (1997).
- ⁵D. Saada, J. Adler, and R. Kalish, *Int. J. Mod. Phys. C* **9**, 61 (1998).
- ⁶J.P. Goss, B.J. Coomer, R. Jones, T.D. Shaw, P.R. Briddon, M. Rayson, and S. Oberg, *Phys. Rev. B* **63**, 195208 (2001).
- ⁷A. Mattausch, M. Bockstedte, and O. Pankratov, *Mater. Sci. Forum* **389-393**, 481 (2002).
- ⁸A. Gali, P. Deák, N.T. Son, and E. Janzén, *Mater. Sci. Forum* **389-393**, 477 (2002).
- ⁹J. Walker, *J. Phys. C* **10**, 3867 (1977).
- ¹⁰M.E. Newton, B.A. Campbell, D.J. Twitchen, J.M. Baker, and T.R. Anthony, *Diamond Relat. Mater.* **11**, 618 (2002).
- ¹¹J.W. Steeds, S. Charles, T.J. Davis, A. Gilmore, J. Hayes, D. Pickard, and J.E. Butler, *Diamond Relat. Mater.* **8**, 94 (1999).
- ¹²L. Allers, A.T. Collins, and J. Hiscock, *Diamond Relat. Mater.* **7**, 228 (1998).
- ¹³G. Davies, H. Smith, and H. Kanda, *Phys. Rev. B* **62**, 1528 (2000).
- ¹⁴J. Kulda, B. Dorner, B. Roessli, H. Sterner, R. Bauer, T. May, K. Karch, P. Pavone, and D. Strauch, *Solid State Commun.* **99**, 799 (1996).
- ¹⁵G. Davies, B. Campbell, A. Mainwood, M.E. Newton, M. Watkins, H. Kanda, and T.R. Anthony, *Phys. Status Solidi A* **186**, 187 (2001).
- ¹⁶S.J. Breuer and P.R. Briddon, *Phys. Rev. B* **51**, 6985 (1995).
- ¹⁷A.A. Kaplyanskii, *Opt. Spectrosc.* **16**, 329 (1964).
- ¹⁸S.C. Lawson, G. Davies, A.T. Collins, and A. Mainwood, *J. Phys.: Condens. Matter* **4**, 3439 (1992).
- ¹⁹R. Vogelgesang, A.K. Ramdas, S. Rodriguez, M. Grimsditch, and T. Anthony, *Phys. Rev. B* **54**, 3989 (1996).
- ²⁰F.S. Ham, *Phys. Rev.* **138**, A1727 (1965).
- ²¹J.P. Goss, R. Jones, and P.R. Briddon, *Phys. Rev. B* **65**, 035203 (2002).
- ²²A. M. Mainwood and K. Johnston (private communication).
- ²³A. Gali, P. Deák, P. Ordejón, N.T. Son, E. Janzén, and W.J. Choyke, *Phys. Rev. B* **68**, 125201 (2003).
- ²⁴G. Davies, T. Gregorkiewicz, M.Z. Iqbal, M. Kleverman, E.C. Lightowlers, N.Q. Vinh, and M. Zhu, *Phys. Rev. B* **67**, 235111 (2003).